Chapter 10

Neutrino oscillations: a phenomenological overview

GianLuigi Fogli
Dipartimento di Fisica e INFN, Sezione di Bari, Via Amendola 173, 70126 Bari, Italy

The evidence for solar and atmospheric neutrino oscillations is analysed in a three-flavour oscillation framework, including the most recent Super-Kamiokande data, as well as the constraints on ν_e mixing coming from the CHOOZ reactor experiment. The regions of the mass-mixing parameter space compatible with the data are determined and their features discussed. In particular, it is shown that bimaximal mixing (or nearly bimaximal mixing) of atmospheric and solar neutrinos is also possible within the MSW solution to the solar neutrino problem.

10.1 Introduction

The recent atmospheric neutrino data from the Super-Kamiokande (SK) experiment [1] are in excellent agreement with the hypothesis of flavour oscillations in the $\nu_\mu \leftrightarrow \nu_\tau$ channel [2]. Such a hypothesis is consistent with all the SK data, including sub-GeV e-like and μ-like events (SGe, μ), multi-GeV e-like and μ-like events (MGe, μ), and upward-going muon events (UPμ), and is also corroborated by independent atmospheric neutrino results from the MACRO [3] and Soudan-2 [4] experiments. Oscillations in the $\nu_\mu \leftrightarrow \nu_\tau$ channel are also compatible with the negative results of the reactor experiment CHOOZ in the $\nu_e \leftrightarrow \nu_e$ channel [5, 6].

However, *dominant* $\nu_\mu \leftrightarrow \nu_\tau$ transitions plus *subdominant* $\nu_\mu \leftrightarrow \nu_e$ transitions are also consistent with SK+CHOOZ data, and lead to a much richer three-flavour oscillation phenomenology for atmospheric νs [7]. A three-flavour framework is also needed in order to accommodate, in addition, the evidence for solar ν_e disappearance [8].

In this chapter we analyse atmospheric and solar data in a common 3ν oscillation framework. Concerning atmospheric νs, we include 30 data points from the SK experiment (52 kTy) [1], namely the zenith distributions of sub-GeV events (SG e-like and μ-like, $5+5$ bins), multi-GeV events (MGe, μ $5+5$ bins) and upward-going muons (UPμ, 10 bins). We also include, when appropriate, the rate of events in the CHOOZ reactor experiment (one bin). Concerning solar neutrinos, we use the total rate information from the Homestake (chlorine), GALLEX+SAGE (gallium), Kamiokande and Super-Kamiokande experiments, as well as the day–night asymmetry and the 18-bin energy spectrum from Super-Kamiokande (825 days) [1], with emphasis on the Mikheyev–Smirnov–Wolfenstein solutions.

10.2 Three-neutrino mixing and oscillations

The combined sources of evidence for neutrino flavour transitions coming from the solar ν problem and from the atmospheric ν anomaly demand an approach in terms of three-flavour oscillations among massive neutrinos (ν_1, ν_2, ν_3) [7–9]. The three-flavour ν parameter space is then spanned by six variables:

$$\delta m^2 = m_2^2 - m_1^2, \tag{10.1}$$

$$m^2 = m_3^2 - m_2^2, \tag{10.2}$$

$$\omega = \theta_{12} \in [0, \pi/2], \tag{10.3}$$

$$\phi = \theta_{13} \in [0, \pi/2], \tag{10.4}$$

$$\psi = \theta_{23} \in [0, \pi/2], \tag{10.5}$$

$$\delta = CP \text{ violation phase}, \tag{10.6}$$

where the θ_{ij} rotations are conventionally ordered as for the quark mixing matrix [10].

In the phenomenologically interesting limit $|\delta m^2| \ll |m^2|$, the two eigenstates closest in mass (ν_1, ν_2) are expected to drive solar ν oscillations, while the 'lone' eigenstate ν_3 drives atmospheric ν oscillations. In such a limit (see [7–10] and references therein) the following occur:

(i) the phase δ becomes unobservable;
(ii) the atmospheric parameter space is spanned by (m^2, ψ, ϕ); and
(iii) the solar ν parameter space is spanned by $(\delta m^2, \omega, \phi)$.

In other words, in the previous limit it can be shown that solar neutrinos probe the composition of ν_e in terms of mass eigenstates

$$\nu_e = U_{e1}\nu_1 + U_{e2}\nu_2 + U_{e3}\nu_3 \tag{10.7}$$

$$= c_\phi(c_\omega \nu_1 + s_\omega \nu_2) + s_\phi \nu_3 \tag{10.8}$$

in the parameter space

$$(\delta m^2, \omega, \phi) \equiv (\delta m^2, U_{e1}^2, U_{e2}^2, U_{e3}^2), \tag{10.9}$$

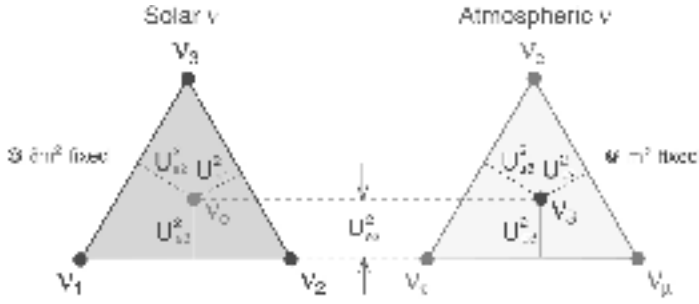

Figure 10.1. Parameter spaces of solar and atmospheric neutrinos in the limit $|\delta m^2| \ll |m^2|$, for assigned δm^2 and m^2. The only common parameter is $U_{e3}^2 = s_\phi^2$.

where $U_{e1}^2 + U_{e2}^2 + U_{e3}^2 = 1$ for unitarity, whereas atmospheric (more generally, 'terrestrial') neutrinos probe the flavour composition of ν_3,

$$\nu_3 = U_{e3}\nu_e + U_{\mu 3}\nu_\mu + U_{\tau 3}\nu_\tau \tag{10.10}$$

$$= s_\phi \nu_e + c_\phi(s_\psi \nu_\mu + c_\psi \nu_\tau) \tag{10.11}$$

in the parameter space

$$(m^2, \psi, \phi) \equiv (m^2, U_{e3}^2, U_{\mu 3}^2, U_{\tau 3}^2), \tag{10.12}$$

where $U_{e3}^2 + U_{\mu 3}^2 + U_{\tau 3}^2 = 1$ for unitarity. The two unitarity constraints can be conveniently embedded [9] in two triangle plots (see figure 10.1), which describe the mixing parameter spaces for given δm^2 and m^2 for solar and atmospheric neutrinos, respectively. The only parameter common to the two triangles is $U_{e3}^2 = s_\phi^2$†.

10.3 Analysis of the atmospheric data

In this section we report an updated analysis of the Super-Kamiokande data, and combine them with the limits coming from the CHOOZ reactor experiment, by assuming the 'standard' three-neutrino framework discussed in the previous section. Details about our calculations can be found in [7]. Constraints on the mass-mixing parameters are obtained through a χ^2 statistics, and are plotted in the atmospheric ν triangle described in figure 10.1.

Figure 10.2 shows the regions favoured at 90% and 99% C.L. in the triangle plots, for representative values of m^2. The CHOOZ data, which exclude a large horizontal strip in the triangle, appear to be crucial in constraining three-flavour mixing. Pure $\nu_\mu \leftrightarrow \nu_e$ oscillations (right-hand side of the triangles) are excluded

† In the special case $\phi = 0$, the atmospheric and solar parameter spaces are decoupled into the two-family oscillation spaces $(\delta m^2, \omega)$ and (m^2, ψ).

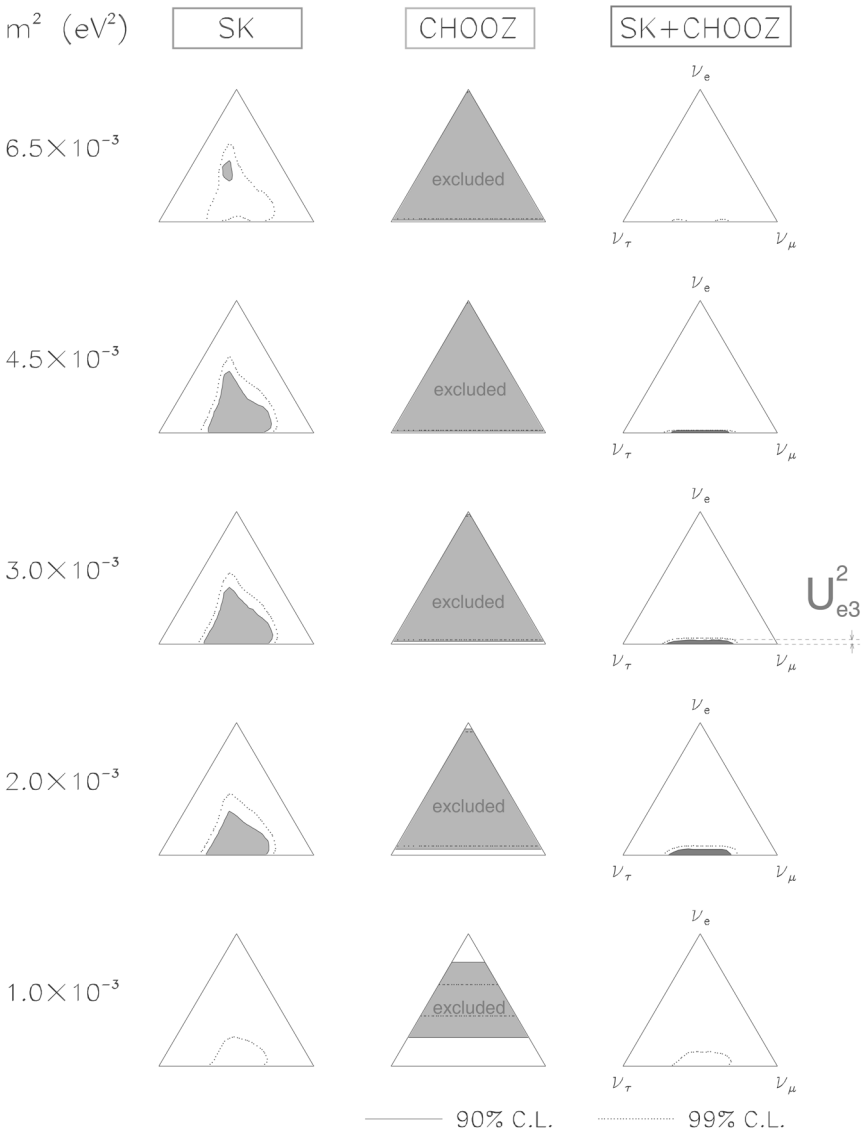

Figure 10.2. Three-flavour analysis in the triangle plot, for five representative values of m^2. Left-hand and middle column: separate analyses of Super-Kamiokande (52 kTy) and CHOOZ data, respectively. Right-hand column: combined SK+CHOOZ allowed regions. Although the SK+CHOOZ solutions are close to pure $\nu_\mu \leftrightarrow \nu_\tau$ oscillations, the allowed values of U^2_{e3} are not completely negligible, especially in the lower range of m^2.

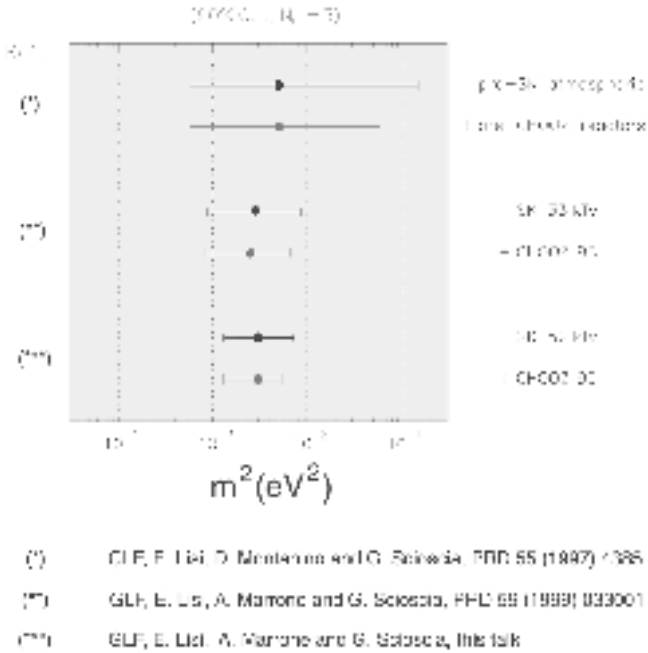

Figure 10.3. 90% C.L. bounds on the mass parameter m^2 from atmospheric data, without and with reactor data. Upper part: pre-SK and pre-CHOOZ bounds. Intermediate part: SK bounds at 32 kTy (+CHOOZ). Lower part: present bounds from SK data at 52 kTy (+CHOOZ).

by SK and CHOOZ independently. The centre of the lower side, corresponding to pure $\nu_\mu \leftrightarrow \nu_\tau$ oscillations with maximal mixing, is allowed in each triangle both by SK and SK+CHOOZ data. However, deviations from maximal ($\nu_\mu \leftrightarrow \nu_\tau$) mixing, as well as subdominant mixing with ν_e, are also allowed to some extent. Such deviations from maximal 2ν mixing are now more constrained than in the previous analysis of the 33 kTy SK data [7], also as a result of tighter constraints from the finalized CHOOZ data [5].

Figure 10.3 shows the progressively tighter constraints on the mass parameter m^2 for unconstrained three-flavour mixing, for pre-SK [11] and post-SK [7] analyses, with and without reactor constraints. The current best-fit value (lower part of figure 10.3) is reached at $m^2 \sim 3 \times 10^{-3}$ eV^2, and is only slightly influenced by the inclusion of CHOOZ data. However, the upper bound on m^2 is significantly improved by including CHOOZ. Note that there is consistency between pre-and post-SK information.

Figures 10.2 and 10.3 clearly show the tremendous impact of the SK experiment in constraining the neutrino oscillation parameter space. Prior to SK, the data could not significantly favour $\nu_\mu \leftrightarrow \nu_\tau$ over $\nu_\mu \leftrightarrow \nu_e$ oscillations, and

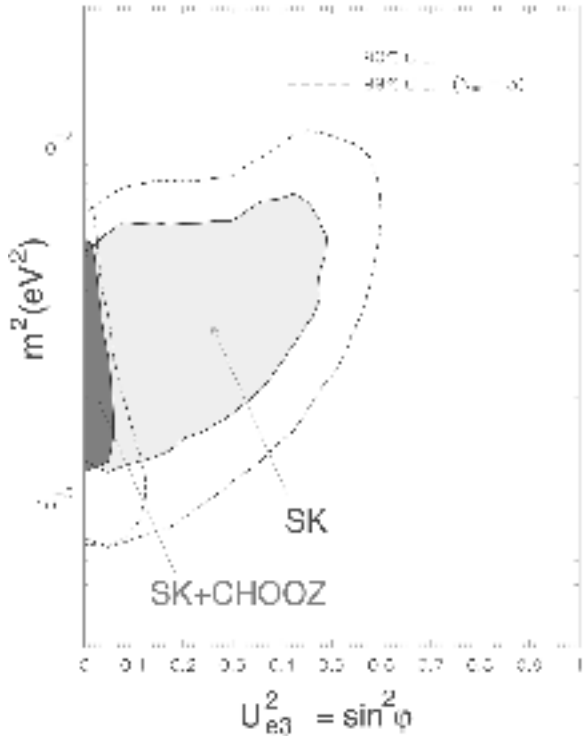

Figure 10.4. Bounds on U^2_{e3} as a function of m^2 from SK data (52 kTy), with and without the finalized CHOOZ data.

could only put relatively weak bounds on m^2 (see [11]).

The impact of CHOOZ in constraining the mixing matrix element U^2_{e3} is clearer in figure 10.4, where the 90% and 99% C.L. bounds are shown as a function of m^2, for unconstrained values of the angle ψ. It can be seen that, when CHOOZ data are included, the element U^2_{e3} cannot be larger than a few percent.

Figure 10.5 shows the best-fit zenith distributions of SGe, μ, MGe, μ and UPμ events, normalized to the no-oscillation rates in each bin, with and without the CHOOZ constraint. The non-zero value of U^2_{e3} at the best-fit point (SK data only) leads to a slight expected excess in the MGe sample for $\cos\theta \to -1$. A significant reduction in the errors is needed to probe such possible distortions, which would be unmistakable signals of subdominant $\nu_\mu \to \nu_e$ oscillations. Figure 10.5 also shows that, when the results of CHOOZ are included, pure $\nu_\mu \to \nu_\tau$ oscillations represent the best fit to the SK data. In this context, it is useful to show that the pieces of information coming from the *shape* of the zenith distributions (figure 10.5) and from the total event rates are consistent with

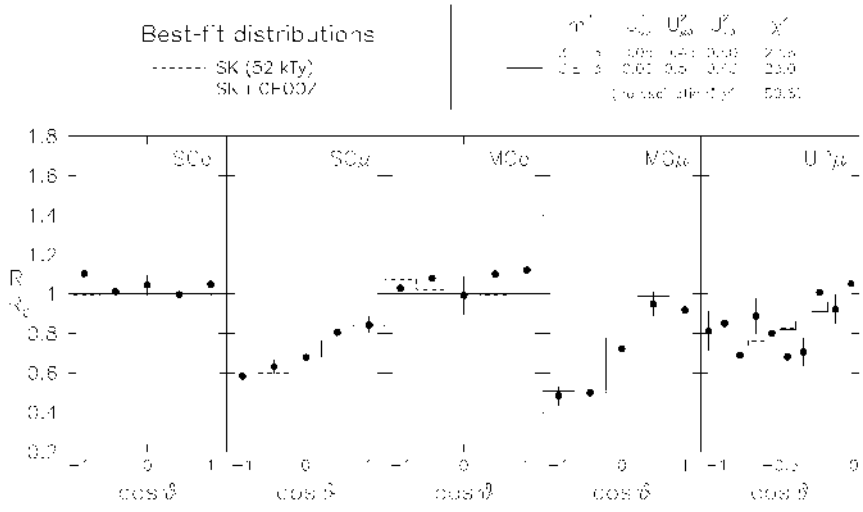

Figure 10.5. SK zenith distributions of leptons at best fit (broken lines), also including CHOOZ (full lines), as compared with the 52 kTy experimental data (dots with error bars). The 3ν mass-mixing values at best fit are indicated in the upper right-hand corner.

each other, contrary to recent claims [12].

To this purpose, figure 10.6 shows the curve of theoretical predictions for maximal 2ν mixing ($U^2_{\mu 3} = U^2_{\tau 3}$ and $U^2_{e3} = 0$) and variable m^2, in the plane of the double ratio of μ-to-e events for SG and MG events, together with the SK data (cross of error bars). The SK data on the double ratio, within one standard deviation, are perfectly consistent with the $\nu_\mu \to \nu_\tau$ oscillation hypothesis at $m^2 \sim 3 \times 10^{-3}$ eV^2.

10.4 Analysis of the solar data

10.4.1 Total rates and expectations

In this section we present an updated phenomenological analysis of the solar neutrino data, assuming oscillations between two and three neutrino families, with emphasis on the MSW [13] solutions.

As far as expectations are concerned, we use the so-called BP98 standard solar model [14] for the electron density in the Sun and for the input neutrino parameters (ν_e fluxes, spectra, and production regions), and compare the predictions to the experimental data for the following observables: total neutrino event rates, SK energy spectrum and SK day–night asymmetry.

The total neutrino event rates are those measured at Homestake [15], Kamiokande [16], SAGE [17], GALLEX [18], and Super-Kamiokande (825 live days) [1]. Since the SAGE and GALLEX detectors measure the same quantity

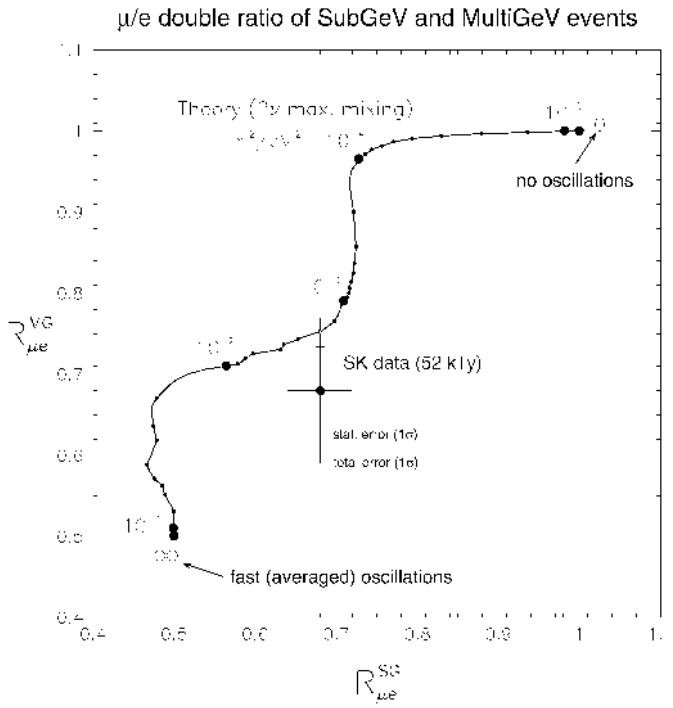

Figure 10.6. Double ratio of μ/e events (data/theory) for SG and MG events in SK: full curve, predictions for maximal $\nu_\mu \to \nu_\tau$ mixing; cross, SK data ($\pm 1\sigma$).

their results are combined in a single (Ga) rate. The Kamiokande and SK data, however, are treated separately (rather than combined in a single datum), since the two experiments, although based on the same ν–e scattering detection technique, have rather different energy thresholds and resolution functions.

The SK electron recoil energy spectrum and its uncertainties (825 lifetime days, $E_e > 5.5$ MeV) are graphically reduced from the 18-bin histograms shown by SK members in recent Summer '99 conferences [1]. Our theoretical calculation of the binned spectrum properly takes into account energy threshold and resolution effects. Standard ^{8}B [19] and *hep* [14] neutrino spectra and fluxes are used, unless otherwise noted. Concerning the SK day–night asymmetry of the event rates, we use the latest measurement [1]: $2(N - D)/(N + D) = 0.065 \pm 0.031 \pm 0.013$.

In the presence of 2ν or 3ν oscillations, the MSW effect in the Sun is computed as in [9]. The additional Earth matter effects are treated as in [20]. The χ^2 analysis basically follows the approach developed in [21, 22], with the necessary updates to take into account the BP98 SSM predictions and the energy spectrum information. Further details can be found in [23].

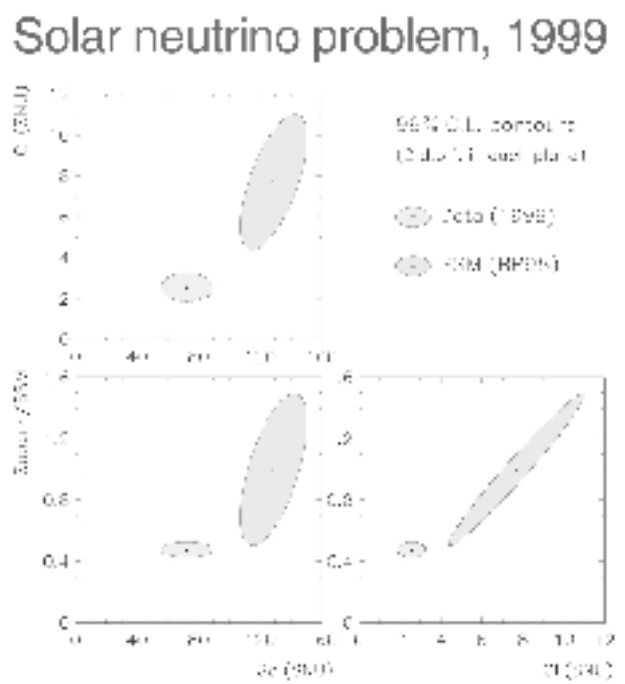

Figure 10.7. The solar neutrino deficit, shown as a discrepancy between data and expectations in the gallium (Ga), chlorine (Cl), and Super-Kamiokande total event rates. In each plane, the error ellipses represent 99% C.L. contours for two degrees of freedom (i.e. $\Delta\chi^2 = 9.21$). The projection of an ellipse onto one of the axis gives approximately the $\pm 3\sigma$ range for the corresponding rate.

We start our analysis by comparing the standard (no oscillation) predictions with the experimental data for the Cl, Ga, and SK total rates. Figure 10.7 shows the 99% C.L. error ellipses for data and expectations in the planes charted by the (Cl, Ga), (SK, Ga) and (SK, Cl) total rates. The distance between observations and standard predictions makes the solar ν problem(s) evident. At present, such information is the main evidence for solar neutrino physics beyond the standard electroweak model; however, since the theoretical errors are dominant—as far as total rates are concerned—no substantial improvements can be expected by a reduction in the experimental errors. Conversely, decisive information is expected from the SK spectrum and day–night asymmetry, but no convincing deviation has emerged from such data yet. Therefore, it is not surprising that, in oscillation fits, the total rates mainly determine *allowed* regions, while the SK spectrum and day–night asymmetry determine *excluded* regions.

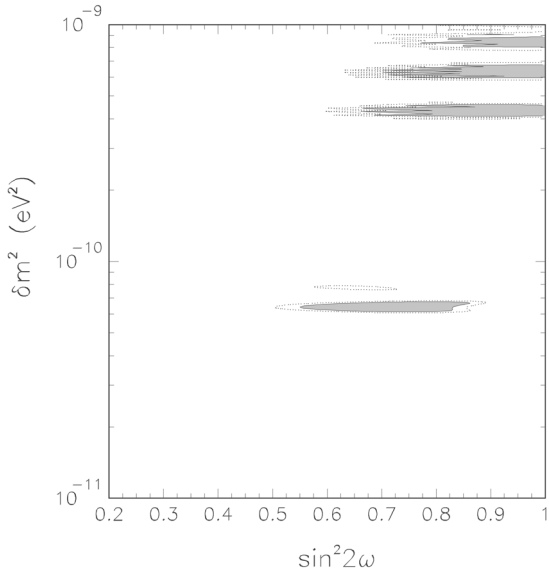

Figure 10.8. Two-generation vacuum solutions to the solar neutrino problem (all data included). Upper solutions fit the SK spectrum better than total rates. Conversely, the solution at lowest δm^2 fits the total rates (Cl + Ga + K + SK) better.

10.4.2 Two-flavour oscillations in vacuum

In figure 10.8 we report our 2ν vacuum oscillation analysis of the solar neutrino data coming from total rates end SK electron energy spectrum. We can see several distinct solutions, allowed at the 90% C.L., with the peculiar behaviour that in general a certain disagreement can be found by a comparison of the total rates and energy spectrum constraints. There are solutions which are preferred by the total rates analysis, but disfavoured by the energy spectrum, and solutions that, conversely, are mainly indicated by the energy spectrum but not by total rates. This behaviour has also been noted in [24]. An interesting feature is that, if one of the vacuum solutions is selected by future data, then we will be able to determine the mass difference δm^2 in a very accurate way.

10.4.3 Two-flavour oscillations in matter

Figure 10.9 shows the results of our 2ν MSW analysis of the solar ν data, shown as C.L. contours in the $(\delta m^2, \sin^2 2\omega/\cos 2\omega)$ plane. The choice of the variable $\sin^2 2\omega/\cos 2\omega$, rather than the usual $\sin^2 2\omega$, allows an expanded view of the large mixing region.

In each of the six panels, we determine the absolute minimum of the χ^2 and then plot the iso-χ^2 contours corresponding to 90%, 95% and 99% C.L. for

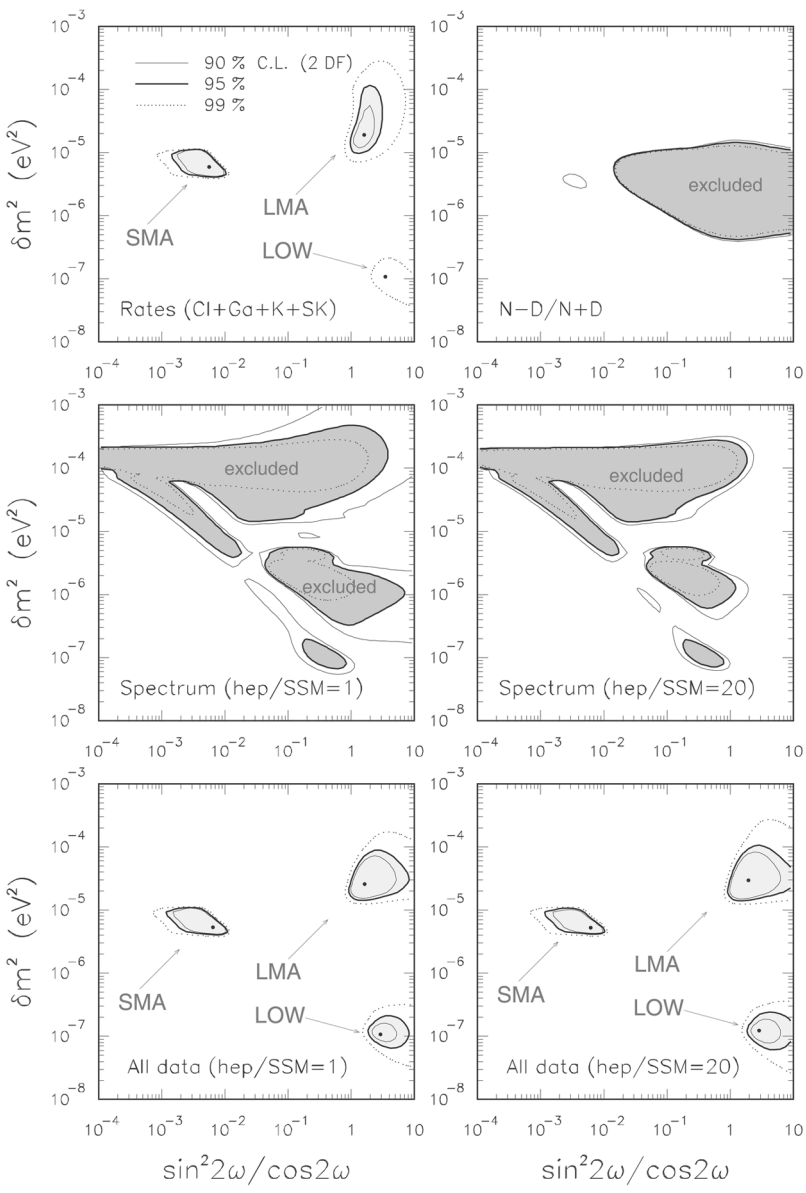

Figure 10.9. Two-generation MSW solutions to the solar neutrino problem. The upper four panels correspond to the following separate fits to data subsets: total rates (Cl + Ga + K + SK); Super-Kamiokande night–day asymmetry $N - D/N + D$; Super-Kamiokande electron energy spectrum with standard *hep* neutrino flux; Super-Kamiokande spectrum with enhanced (20×) *hep* neutrino flux. The two lower panels show the results of the global fits to all data.

two degrees of freedom (the oscillation parameters). In fits including the total rates, there is a global χ^2 minimum and two local minima; such minima, and the surrounding favoured regions, are usually indicated as MSW solutions at small mixing angle (SMA), large mixing angle (LMA), and low δm^2 (LOW).

The first panel of figure 10.9 refers to the fit to the total rates only. The three χ^2 minima are indicated by dots. The absolute minimum is reached within the SMA solution ($\chi^2_{\min} = 1.08$): it represents a very good fit to the data. The LMA solution is also acceptable, while the LOW solution gives a marginal fit.

The SK data on the day–night asymmetry (second panel) and energy spectrum (third panel) exclude large regions in the mass-mixing parameter space; but are unable to (dis)prove any of the three solutions, which in fact are also present in the global fit to all data (fifth panel).

The spectrum information is sensitive to the (uncertain) value of the *hep* neutrino flux; for instance, an enhancement by a factor 20 helps to fit the high-energy part of the SK spectrum [25], and thus it produces a reduction in the excluded regions in the mass-mixing plane (fourth panel in figure 10.9), and a corresponding slight enlargement of the globally allowed regions (sixth panel).

From a careful analysis [23], the following situation emerges for the three MSW solutions SMA, LMA, and LOW. None of them can be excluded at 99% C.L. by the present experimental data. Different pieces of the data give indications that are not as consistent as would be desirable: the total rate information favours the SMA solution, the spectral data favour the LMA and LOW solutions, and the day–night data favour the LMA solution. In a global fit, the three solutions have comparable likelihoods. Although such solutions are subject to change shape and likelihood as more accurate experimental data become available, no dramatic improvement can be really expected in their selection, unless

(1) the theoretical uncertainties on the total rates are reduced to the size of the corresponding experimental uncertainties;
(2) the total errors associated with the SK spectrum and day–night measurement are significantly reduced (by, say, a factor $\sim$2); or
(3) decisive results are found in new generation solar neutrino experiments. Any of these conditions require a time scale of a few years at least; the same time scale should then be expected in order to (patiently) single out one of the three MSW solutions (SMA, LMA, or LOW).

Another aspect of the LMA and LOW solutions emerging from figure 10.9 is their extension to large values of the mixing angle ($\sin^2 2\omega \to 1$), which are often assumed to be realized only through the vacuum oscillation solutions. Since the possibility of nearly maximal (ν_1, ν_2) mixing for solar neutrinos has gained momentum after the SK evidence for maximal (ν_μ, ν_τ) mixing ($\sin^2 2\psi \sim 1$), it is interesting to study it in detail by dropping the usual '2ω' variable and by exploring the full range $\omega \in [0, \pi/2]$, as was done earlier in [9]. The subcase $\omega = \pi/4$ will receive special attention in the next section.

10.4.4 Three-flavour oscillations in matter

As stated in section 10.2, for large values of m^2 ($\gg 10^{-4}$ eV^2) the parameter space relevant for 3ν solar neutrino oscillations is spanned by the variables $(\delta m^2, \omega, \phi)$. As far as ω is taken in its full range $[0, \pi/2]$, one can assume $\delta m^2 > 0$, since the MSW physics is invariant under the substitution $(\delta m^2, \omega) \rightarrow (-\delta m^2, \pi/2 - \omega)$ at any ϕ.

For graphical representations, we prefer to use the mixing variables ($\tan^2\omega$, $\tan^2\phi$) introduced in [9], which properly chart both small and large mixing. The case $\tan^2\phi = 0$ corresponds to the familiar 2ν scenario, except that now we also consider the usually neglected case $\omega > \pi/4$ ($\tan^2\omega > 1$). For each set of observables (rates, spectrum, day-night difference, and combined data) we compute the corresponding MSW predictions and their uncertainties, identify the absolute minimum of the χ^2 function, and determine the surfaces at $\chi^2 - \chi^2_{\rm min} = 6.25$, 7.82 and 11.36, which define the volumes constraining the $(\delta m^2, \tan^2\omega, \tan^2\phi)$ parameter space at 90%, 95% and 99% C.L. Such volumes are graphically presented in $(\delta m^2, \tan^2\omega)$ slices for representative values of $\tan^2\phi$.

Figure 10.10 shows the combined fit to all data. The minimum χ^2 is reached within the SMA solution and shows a very weak preference for non-zero values of ϕ ($\tan^2\phi \simeq 0.1$). It can be seen that the SK spectrum excludes a significant fraction of the solutions at $\delta m^2 \sim 10^{-4}$ eV^2, including the upper part of the LMA solution at small ϕ, and the merging with the SMA solution at large ϕ. In particular, at $\tan^2\phi = 0.1$ the 95% C.L. upper limit on δm^2 drops from 2×10^{-4} eV^2 (rates only) to 8×10^{-5} eV^2 (all data). This indication tends to disfavour neutrino searches of *CP* violation effects, since such effects decrease with $\delta m^2/m^2$ at $\phi \neq 0$.

The 95% C.L. upper bound on ϕ coming from solar neutrino data alone ($\phi < 55°$–$59°$) is consistent with the one coming from atmospheric neutrino data alone ($\phi < 45°$), as well as with the upper limit coming from the combination of CHOOZ and atmospheric data ($\phi < 15°$) (see figure 10.4). This indication supports the possibility that solar, atmospheric and CHOOZ data can be interpreted in a single three-flavour oscillation framework [7, 23]. In this case, the CHOOZ constraints on ϕ exclude a large part of the 3ν MSW parameter space (basically all but the first two panels in figure 10.9).

However, even small values of ϕ can be interesting for solar ν phenomenology. Figure 10.11 shows the section of the volume allowed in the 3ν MSW parameter space, for $\omega = \pi/4$ (maximal mixing), in the mass-mixing plane $(\delta m^2, \sin^2\phi)$. All data are included. It can be seen that both the LMA and LOW solutions are consistent with maximal mixing (at 99% C.L.) for $\sin^2\phi \equiv U^2_{\rm e3} = 0$. Moreover, the consistency of the LOW solution with maximal mixing improves significantly for $U^2_{\rm e3} \simeq 0.1$, while the opposite happens for the LMA solution. This gives the possibility of obtaining nearly bimaximal mixing ($\omega = \psi = \pi/4$ with ϕ small) within the LOW solution to the solar neutrino problem—an interesting possibility for models predicting large mixing angles.

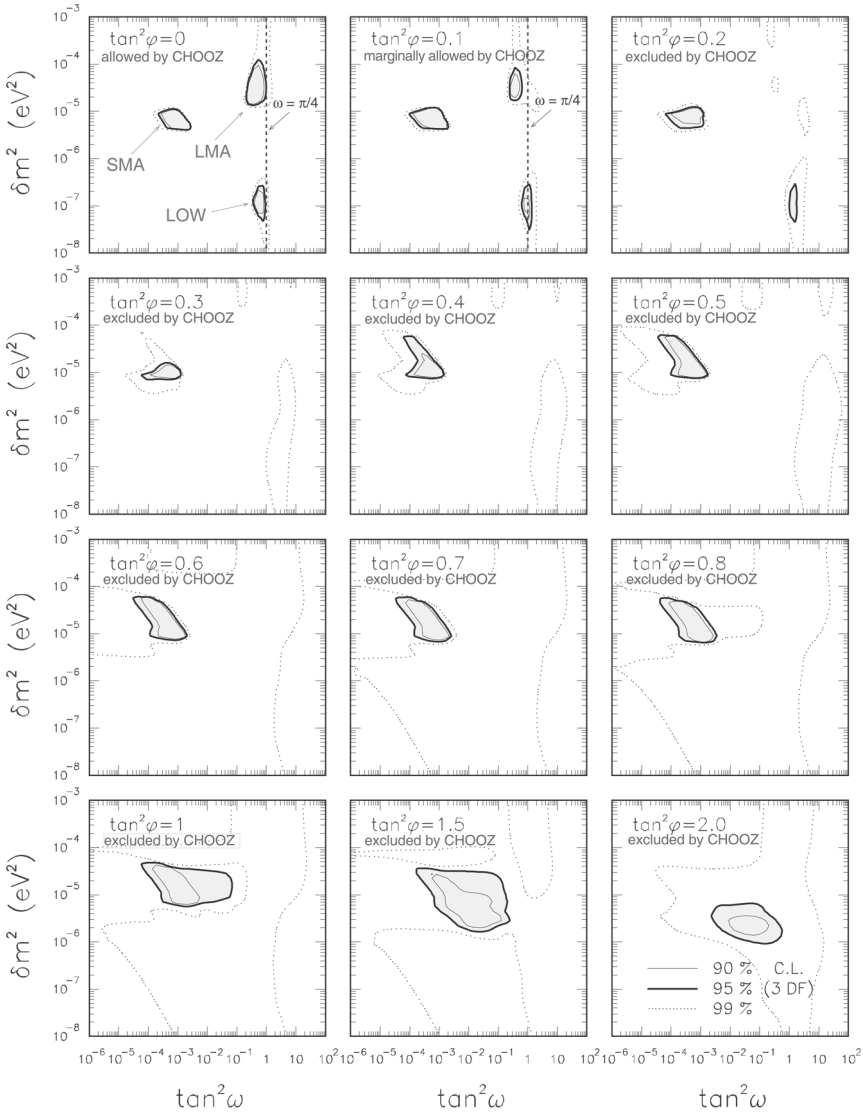

Figure 10.10. Results of the global three-flavour MSW fit to all data. Note that, in the first two panels, the 99% C.L. contours are compatible with maximal mixing ($\tan^2\omega = 1$) for both the LOW and the LMA solutions. Note that, when the CHOOZ constraints on ϕ are included, only the first two panels are permissible (see figure 10.4).

10.5 Conclusions

We have analysed the most recent experimental evidence for solar and atmospheric ν oscillations in a common theoretical framework including three-

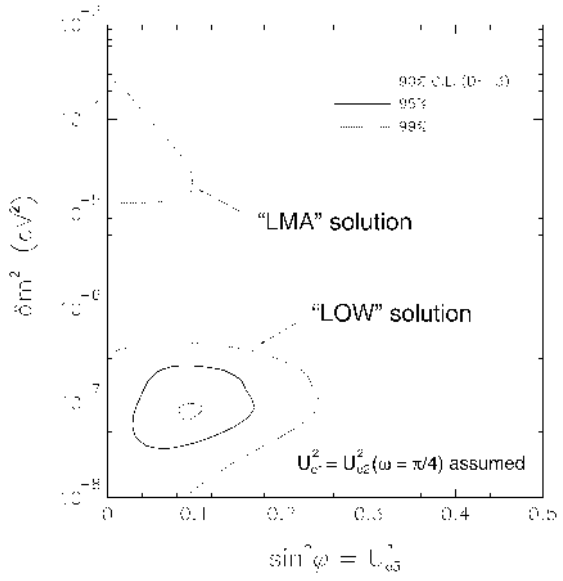

Figure 10.11. Allowed regions in the plane $(\delta m^2, \sin^2\phi)$, assuming maximal (ν_1, ν_2) mixing ($\omega = \pi/4$). For $\sin^2\phi = 0$, both the LMA and LOW solutions are compatible with maximal mixing at 99% C.L. For small values of $\sin^2\phi$, the maximal mixing case favours the LOW solution.

flavour transitions. We have investigated the regions of the mass-mixing parameter space compatible with the data, with and without the CHOOZ constraints. Such regions are of interest both for model-building and as a guidance for future experimental tests. It turns out that both atmospheric and solar ν data prefer low values of the matrix element U_{e3}^2 even without the inclusion of reactor constraints, which represents a non-trivial consistency check.

The addition of CHOOZ data implies the further restriction $U_{e3}^2 <$ few %. Even within such limits, a novel feature emerges from the 3ν MSW analysis of solar neutrinos [23]: bimaximal mixing of atmospheric and solar νs, usually studied in terms of vacuum solar ν solutions, is possible also within the LMA and LOW MSW solutions.

Acknowledgments

The author would like to thank the organizers of the School in 'Contemporary Relativity and Gravitational Physics' for their kind hospitality. This work is co-financed by the Italian Ministero dell'Università e della Ricerca Scientifica e Tecnologica (MURST) within the 'Astroparticle Physics' project.

References

[1] Kajita T 2000 *Nucl. Phys. B (Proc. Suppl.)* **85** 44
[2] Super-Kamiokande Collaboration 1998 *Phys. Rev. Lett.* **81** 1562
[3] Macro Collaboration 1998 *Phys. Lett.* B **434** 451
[4] Soudan 2 Collaboration 2000 *Nucl. Phys. Proc. Suppl.* **91** 134
[5] CHOOZ Collaboration 1999 *Phys. Lett.* B **466** 415
[6] Mikaelyan L 2000 *Nucl. Phys. B (Proc. Suppl.)* **87** 284
[7] Fogli G L, Lisi E Marrone A and Scioscia G 1999 *Phys. Rev.* D **59** 033001
[8] Fogli G L, Lisi E and Montanino D 1994 *Phys. Rev.* D **49** 3626
[9] Fogli G L, Lisi E and Montanino D 1996 *Phys. Rev.* D **54** 2048
[10] Kuo T K and Pantaleone J 1989 *Rev. Mod. Phys.* **61** 937
[11] Fogli G L, E Lisi, D Montanino and G Scioscia 1997 *Phys. Rev.* D **55** 4385
[12] LoSecco J M *Preprint* hep-ph/9807359
J M LoSecco *Preprint* hep-ph/9807432
[13] Wolfenstein L 1978 *Phys. Rev.* D **17** 2369
Mikheyev S P and Smirnov A Yu 1986 *Nuovo Cimento* C **9** 17
[14] Bahcall J N, Basu S and Pinsonneault M 1998 *Phys. Lett.* B **433** 1
See also J N Bahcall's homepage, www.sns.ias.edu/∼jnb
[15] Homestake Collaboration 1998 *Astrophys. J.* **496** 505
[16] Kamiokande Collaboration 1996 *Phys. Rev. Lett.* **77** 1683
[17] SAGE Collaboration 1999 *Phys. Rev.* C **60** 055801
[18] GALLEX Collaboration 1999 *Phys. Lett.* B **447** 127
[19] Bahcall J N *et al* 1996 *Phys. Rev.* C **54** 411
[20] Lisi E and Montanino D 1997 *Phys. Rev.* D **56** 1792
[21] Fogli G L and Lisi E 1994 *Astropart. Phys.* **2** 91
[22] Gonzalez Garcia M C 2000 *Nucl. Phys.* B **573** 3
[23] Fogli G L, Lisi E, Montanino D, and Palazzo A 2000 *Phys. Rev.* D **62** 013002
[24] Bahcall J N, Krastev P I and Smirnov A Yu 2000 *Phys. Lett.* B **477** 401
[25] Bahcall J N and Krastev P I 1998 *Phys. Lett.* B **436** 243